Chiral front propagation in liquid-crystalline materials: Formation of the planar monodomain twisted plywood architecture of biological fibrous composites

Gino De Luca and Alejandro D. Rey*
Department of Chemical Engineering, McGill University, 3610 University Street, Montreal, Quebec, Canada H3A 2B2
(Received 6 November 2002; published 30 January 2004)

Biological fibrous composites commonly exhibit an architecture known as twisted plywood, which is similar to that of the cholesteric liquid-crystalline mesophases. The explanation for the structural similarity is that biological fibrous composites adopt a lyotropic cholesteric liquid-crystalline phase during their formation process. In this work, a mathematical model based on the Landau–de Gennes theory of liquid crystals has been developed to reproduce the process by which long chiral fibrous molecules form the twisted plywood structures observed in biological composites. The dynamics of the process was then further investigated by analytically solving a simplified version of the governing equations. Results obtained from the model are in good qualitative agreement with the theory of Neville [*Biology of Fibrous Composites* (Cambridge University Press, Cambridge, England, 1993)] who hypothesized the necessity of a constraining layer to lock the direction of the helical axis of the plywood in order to create a monodomain structure. Computational results indicate that the plywood architecture is obtained by a chiral front propagation process with a fully relaxed wake. The effects of chirality and concentration on the formation process kinetics are characterized.

DOI: 10.1103/PhysRevE.69.011706 PACS number(s): 61.30.−v, 83.80.Xz, 61.30.Dk, 61.30.St

I. INTRODUCTION

Skeletal and protective extracellular tissues of biological systems are highly organized composite materials [1–7]. They exhibit remarkable mechanical properties but are built from relatively simple constituents such as cellulose, chitin, and collagen [1,7]. In addition, these composite materials are biodegradable and assembled at ambient temperature and pressure in an aqueous environment. Biological composites have therefore undeniable advantages over synthetic materials and are of a growing interest in applied material science. A major challenge in the field is to produce synthetic equivalents of these composite materials. However, to develop a synthetic route, the structural formation process of biological composites needs to be precisely described and understood [6].

Strategies developed by material engineers to solve mechanical problems are often similar to the ones employed by living organisms and even the lower ones [8]. Natural composites exhibit laminated architectures called plywoods [1]. The laminated architecture, the most widely found in nature, is the twisted plywood, also referred as helicoidal plywood [1–7]. The plywood architecture, found in nearly all regular extracellular assemblies of living systems, is well documented in the literature [1–7].

But how are fibrous macromolecules precisely manipulated into the extracellular matrix so as to form the twisted plywood assemblies found in biological composites? The most probable answer is that the extracellular matrix, which surrounds the fibrous water-insoluble molecules, passes through a mobile phase during its development and self-assembly [1–7]. In thermodynamic terms, self-assembly is a free energy minimization process driven by entropy. The free energy of the system is lowered as the excluded volume between the molecules is reduced [8]. Because most naturally occurring biological polymers are chiral—i.e., they are not superimposable on their mirror image—the excluded volume is favorably reduced by twisted/helical packing.

Knowing that natural composites are usually compacted, partially ordered, and required to pass via a more or less fluid state, it is likely that a lyotropic liquid-crystalline phase is involved during their supramolecular self-assembly. Lyotropic liquid-crystalline phases form three-dimensional assemblies, which combine the fluidity of liquids with the long-range orientational order of crystals, above a certain critical concentration of molecules in the solution [9]. Among the different types of liquid-crystalline phases found in nature, cholesteric mesophases demonstrate the greatest structural similarities with the architecture of biological composites. Cholesteric mesophases are three-dimensional assemblies whose molecules lie on a series of equidistant pseudoplanes that are slightly rotated with respect to one another [9]. These mesophases, which are made up of optically active molecules, are characterized by a length scale known as the pitch, p_0, corresponding to the distance required by the molecules to accomplish a 2π radians rotation of their long axis. Figure 1 shows a schematic of the plywood architecture adopted by biological composites (adapted from [3]). The fiberlike constituents display the classical cholesteric or chiral nematic spatial organization defined, in a rectangular (x,y,z) coordinate system, by

$$n_x = \cos\theta(y), \quad n_y = 0, \quad n_z = -\sin\theta(y), \tag{1a}$$

with

$$\theta(y) = \frac{2\pi}{p_0} y, \quad \mathbf{N} = \mathbf{j}, \tag{1b}$$

*Corresponding author. FAX: (514) 398-6678. Electronic address: alejandro.rey@mcgill.ca

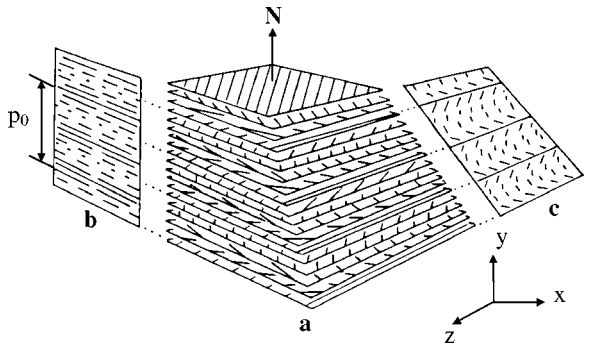

FIG. 1. Schematic representation of the twisted plywood architecture. (a) Parallel and equidistant layers. On each layer, parallel lines indicate the orientation of the fibers. The fibrillar direction rotates by a small constant angle from one layer to the next. (b) Transverse section plane; the fibers appear as dots or segments of different length, all parallel to each other. (c) Oblique section plane; the fibers appear as superposed series of nested arcs. The periodicity seen in these various planes corresponds to a 180° rotation of the fibers. Adapted from [3].

where **n** is the unit vector (director) of the fibers, θ is the angle between the director and the x axis, p_0 is the pitch, **N** is the unit helix vector, and **j** is the unit vector in the y direction. Figure 1(b) presents a schematic of the director field along a plane containing **N** and shows that the fibers rotate continuously along the z direction. Figure 1(c) shows that an oblique cut of the plywood architecture displays arced patterns. The arced patterns are common in biological composites and have been thoroughly characterized by Neville [1]. It is well known that such arced patterns are likely to arise from a cholestericlike organization [1–7].

Despite their similar architectures, cholesteric liquid-crystalline phases and biological fibrous composites present an essential difference. While liquid-crystalline materials exist as a distinct state of matter which is intermediate between a liquid and a solid state, mature biological fibrous composites are in a solid state. The liquid-crystalline character, which is hypothesized to exist during the first steps of the polymer secretion by the cells, is transformed in a solid state by molecular cross-links. However, the imprint of the cholesteric liquid-crystalline phase in the mineralized materials is testified to by the properties of the twisted plywood architecture in electron and polarized-light microscopy [1–5]. Liquid-crystalline theories developed in condensed-matter physics are consequently helpful to advance structural development knowledge for biological fibrous composites.

The mechanical reliability of biological composites resides in their highly hierarchical structure (e.g., molecules, macromolecules, microfibrils, fibrils, fibers, etc.), but also in their twisted plywood architecture [1,4,6,7]. One essential feature of these structures is that they are monodomains [1]. The quasiabsence of defects found in most composites is believed [1] to be due to the presence of a constraining layer that fixes the rotation axis (**N**) of the plywood architecture along the surface unit normal (**j**). Thus knowledge of the conditions under which monodomain defect-free structures are generated is essential to the understanding of biological composites.

Based on these considerations, the specific objectives of this paper are (i) to simulate the ordering process leading to the twisted plywood architecture found in cholesteric liquid-crystalline phases and biological fibrous composites, (ii) to identify the conditions under which the stable defect-free monodomain helicoidal plywood architecture is obtained, and (iii) to characterize the kinetics of the formation process of a monodomain cholesteric liquid crystal and thus predict those of a twisted biological fibrous composite.

This paper is organized as follows. Section II briefly presents the invoked theoretical framework on liquid-crystalline mesophases and the derivation of the governing equations of the model describing the formation of the twisted plywood architecture. Section III is devoted to the computational methods used to solve the model. Section IV presents the computational and analytical results on the plywood architecture formation process. Section V presents the conclusions.

II. THEORY AND GOVERNING EQUATIONS

A. Description of the long-range orientational order

As mentioned above, the structure of liquid-crystalline mesophases is characterized by a long-range orientational order of their constituent molecules. This long-range orientational order is commonly described by a second-order symmetric traceless tensor **Q** corresponding to the second moment of the orientation distribution function. This macroscopic quantity, usually referred as the tensor order parameter, reads [9]

$$\mathbf{Q}=S\left(\mathbf{nn}-\frac{\boldsymbol{\delta}}{3}\right)+\frac{1}{3}P(\mathbf{mm}-\mathbf{l}\cdot\mathbf{l}), \tag{2a}$$

where the following restrictions apply:

$$\mathbf{Q}=\mathbf{Q}^T, \tag{2b}$$

$$\mathrm{tr}(\mathbf{Q})=0, \tag{2c}$$

$$-\frac{1}{2}\leqslant S\leqslant 1, \tag{2d}$$

$$-\frac{3}{2}\leqslant P\leqslant\frac{3}{2}, \tag{2e}$$

$$\mathbf{n}\cdot\mathbf{n}=\mathbf{m}\cdot\mathbf{m}=\mathbf{ll}=1, \tag{2f}$$

$$\mathbf{nn}+\mathbf{mm}+\mathbf{ll}=\boldsymbol{\delta}. \tag{2g}$$

The unit vectors **n**, **m**, and **l** presented in Eqs. (2a), (2f), and (2g) form an orthogonal director triad which characterizes the orientation of the phase. The unit vector **n** is known as the uniaxial director, and **m** and **l** as biaxial directors. The quantities S and P, which are, respectively, known as the uniaxial and biaxial scalar order parameters, are measures of the molecular alignment. The uniaxial scalar order parameter gives the degree of alignment along the uniaxial director **n**, while the biaxial scalar order parameter gives the degree of

alignment along the first biaxial director **m**. The scalar order parameters and the tensor order parameter **Q** (main frame) are given by

$$S=\frac{3}{2}(\mathbf{n}\cdot\mathbf{Q}\cdot\mathbf{n}), \tag{3a}$$

$$P=\frac{3}{2}(\mathbf{m}\cdot\mathbf{Q}\cdot\mathbf{m}-\mathbf{l}\cdot\mathbf{Q}\cdot\mathbf{l}), \tag{3b}$$

$$\mathbf{Q}=\begin{bmatrix} -\frac{1}{3}(S-P) & 0 & 0 \\ 0 & -\frac{1}{3}(S+P) & 0 \\ 0 & 0 & \frac{2}{3}S \end{bmatrix}. \tag{3c}$$

The tensor order parameter **Q** characterizes thoroughly the microstructure of the phase by combining information about orientation and alignment. Its quadrupolar symmetry retains the usual head-tail invariance that implies equivalence between the director field $\mathbf{n}(r)$ and $-\mathbf{n}(r)$. According to Eq. (3) the correspondences between phase and alignment are isotropic $(S=0,P=0)$, uniaxial $(S\neq 0,P=0)$, and biaxial $(S\neq 0,P\neq 0)$.

B. Landau–de Gennes theory of liquid-crystalline materials

The Landau–de Gennes theory expresses the free energy density of the liquid-crystalline material as a power series expansion of scalar invariants of the tensor order parameter **Q** and its gradients $\nabla\mathbf{Q}$ [9] representing short- and long-range elastic effects, respectively. In the absence of external fields, the total free energy density of the mesophase can be given in the following dimensionless form [9,10]:

$$f=f_{\mathrm{is}}+f_{\mathrm{sr}}+f_{\mathrm{lr}}, \tag{4a}$$

$$f_{\mathrm{sr}}=\frac{1}{2}\left(1-\frac{U}{3}\right)\mathrm{tr}(\mathbf{Q}^2)-\frac{U}{3}\mathrm{tr}(Q^3)+\frac{U}{4}[\mathrm{tr}(\mathbf{Q}^2)]^2, \tag{4b}$$

$$f_{\mathrm{lr}}=\frac{1}{2}\left\{\left[\left(\frac{\xi}{h_0}\right)(\nabla\times\mathbf{Q})+4\pi\left(\frac{\xi}{p_0}\right)\mathbf{Q}\right]^2+\upsilon\left[\left(\frac{\xi}{h_0}\right)(\nabla\cdot\mathbf{Q})\right]^2\right\}, \tag{4c}$$

where f_{is} is the free energy density of the isotropic state which depends on conventional thermodynamic parameters, such as temperature, pressure, and concentration. f_{sr} and f_{lr} are, respectively, the short- and long-range contributions to the total free energy density f. The dimensionless parameter U is a thermodynamic potential proportional to the dimensionless concentration of rodlike molecules in the material which drives the isotropic-cholesteric phase transition. The thermodynamic potential U is related to the concentration C by the relation $U=3C/C^*$, where C^* is the concentration at the phase transition. The parameter ξ is a coherence/internal length that gives the distance over which variations of long-range orientational order can occur. This length furnishes the order of magnitude for the size of a defect. The parameter h_0 is an external/geometric length that gives the thickness of the material. The parameter p_0 is the pitch of the cholesteric liquid-crystalline material. It is essential to recognize that this model is therefore of a mesoscopic nature since it includes a molecular (ξ) length scale and a macroscopic (h_0) length scale. The remaining parameter υ represents a measure of the elastic anisotropy of the material. This parameter is constrained to be greater than $-1/2$ in order to ensure the positivity and thermodynamic stability of the long-range contribution to the free energy.

The time evolution of the tensor order parameter **Q** is given by a standard dimensionless gradient flow equation [11,12]:

$$-\gamma(\mathbf{Q})\frac{\partial\mathbf{Q}}{\partial t}=\frac{\delta f}{\delta\mathbf{Q}}=\left[\frac{\partial f}{\partial\mathbf{Q}}-\nabla\cdot\frac{\partial f}{\partial\nabla\mathbf{Q}}\right]^{[s]}, \tag{5a}$$

$$\gamma(\mathbf{Q})=\left(1-\frac{3}{2}\mathrm{tr}(\mathbf{Q}^2)\right)^2, \tag{5b}$$

where the superscript $[s]$ denotes symmetric and traceless tensors, and where $\gamma(\mathbf{Q})$ is a rotational viscosity. Substituting Eqs. (5a) and (5b) into Eqs. (4a), (4b), and (4c) yields the dimensionless governing equation $\mathbf{Q}=\mathbf{Q}(r,t)$ for the time evolution of the tensor order parameter:

$$-\gamma(\mathbf{Q})\frac{\partial\mathbf{Q}}{\partial t}=\mathrm{SR}+\mathrm{LR}, \tag{6a}$$

$$\mathrm{SR}=\left(1-\frac{U}{3}\right)\mathbf{Q}-U(\mathbf{Q}\cdot\mathbf{Q})^{[s]}+U(\mathbf{Q}:\mathbf{Q})\mathbf{Q}, \tag{6b}$$

$$\mathrm{LR}=-\left(\frac{\xi}{h_0}\right)^2\{\nabla^2\mathbf{Q}-[\nabla\cdot(\nabla\mathbf{Q})^T]^{[s]}+\upsilon[\nabla\cdot(\nabla\cdot\mathbf{Q})]^{[s]}\}+\left(\frac{\xi}{h_0}\right)\left(\frac{\xi}{p_0}\right)[-8\pi(\nabla\times\mathbf{Q})]^{[s]}+\left(\frac{\xi}{p_0}\right)^2[-16\pi^2\mathbf{Q}]. \tag{6c}$$

The tensors SR and LR represent the short- and long-range contributions to the dynamics of **Q**. The coupling parameter ξ/h_0 controls the balance between short- and long-range effects while ξ/p_0 controls the balance between chiral and achiral effects. In the limit $\xi/p_0\rightarrow 0$, the material describes an achiral ordinary nematic liquid-crystalline material.

III. COMPUTATIONAL MODELING

In order to understand the process which leads to the planar monodomain twisted plywood architecture observed in the broad majority of biological fibrous composites, we simulate the time evolution of the tensor order parameter **Q** in a lyotropic cholesteric liquid-crystalline material. Since the tensor order parameter has five independent components (symmetric and traceless), five coupled time-dependent nonlinear partial differential equations need to be solve simultaneously. The computational domain is the unit square $(0\leqslant x\leqslant 1,0\leqslant y\leqslant 1)$, and hence $\mathbf{Q}=\mathbf{Q}(x,y,t)$. We emphasize

that, despite the fact that the simulation domain is two dimensional (2D), **Q** conserves its five degrees of freedom.

A. Boundary conditions

In order to restrict the influence of physical boundaries on the material bulk, periodic boundary conditions are employed on the x direction. The boundary conditions adopted on the remaining bounding surfaces are of the Dirichlet type. The upper boundary of the computational domain ($y=1$) describes an isotropic state in order to represent the surface of a secreting cell, as described in [1], and **Q** is defined by Eq. (2a). The lower boundary ($y=0$) corresponds to a crystallized ordered layer. Along this boundary, the molecules describe a strong planar anchoring and accordingly the director triad is given by

$$\mathbf{n}(y=0)=(1\ \ 0\ \ 0), \tag{7a}$$

$$\mathbf{m}(y=0)=(0\ \ 1\ \ 0), \tag{7b}$$

$$\mathbf{l}(y=0)=(0\ \ 0\ \ 1). \tag{7c}$$

The alignment of the molecules along these particular directions is given by the equilibrium scalar order parameter S_{eq} and P_{eq}. These values are determined by the steady-state solutions of the following autonomous nonlinear system of coupled differential equations:

$$\frac{\partial S}{\partial t}=\frac{3}{2}\left(\mathbf{n}\cdot\frac{\partial \mathbf{Q}}{\partial t}\cdot\mathbf{n}\right)$$
$$=\left(-\frac{2}{9}P^2S-\frac{1}{9}P^2+\frac{1}{3}S^2-\frac{2}{3}S^3+\frac{1}{3}S\right)$$
$$\times U-S-4\pi^2\left(\frac{\xi}{p_0}\right)^2(S-P), \tag{8a}$$

$$\frac{\partial P}{\partial t}=\frac{3}{2}\left(\mathbf{m}\cdot\frac{\partial \mathbf{Q}}{\partial t}\cdot\mathbf{m}-\mathbf{l}\cdot\frac{\partial \mathbf{Q}}{\partial t}\cdot\mathbf{l}\right)$$
$$=\left(-\frac{2}{3}S^2P-\frac{2}{3}PS-\frac{2}{9}P^3+\frac{1}{3}P\right)$$
$$\times U-P+12\pi^2\left(\frac{\xi}{p_0}\right)^2(S-P). \tag{8b}$$

Note that we have $\partial\mathbf{n}/\partial t=\partial\mathbf{m}/\partial t=\partial\mathbf{l}/\partial t=0$.

B. Initial conditions

Initially, the liquid-crystalline material is taken to be in a stable isotropic state. This disordered state corresponds to the physical situation of a low concentration of chiral fibrous molecules in the surrounding extracellular matrix of the biological composite. The initial tensor order parameter field $\mathbf{Q}_0=\mathbf{Q}(t=0)$ characterizing the initial microstructure of the material is defined in the following way:

$$\mathbf{Q}_0=S_0\left(\mathbf{e}_1\mathbf{e}_1-\frac{\boldsymbol{\delta}}{3}\right)+\frac{1}{3}P_0(\mathbf{e}_2\mathbf{e}_2-\mathbf{e}_3\mathbf{e}_3), \tag{9}$$

where S_0 and P_0 are random numbers between -1×10^{-10} and 1×10^{-10} representing thermal fluctuations in the degree of order. The random orthogonal unit vectors $\mathbf{e}_1$, $\mathbf{e}_2$, and $\mathbf{e}_3$ describe the initial isotropic orientation of the molecules in the material.

C. Numerical methods

The governing equations are solved using the classical numerical method of lines which consists of transforming the set of governing partial differential equations into a set of ordinary differential equations by spatial discretization and subsequently integrating with respect to time. Since the geometry of the computational domain is trivial, we use second-order finite difference approximations for the spatial derivatives. The mesh refinement technique was performed to confirm the invariance of the results with respect to the grid spacing. Time integration was performed with a Runga-Kutta-Chebyshev algorithm. This explicit method, with an extended domain of stability, possesses an adaptive time-stepping scheme that captures the physics contained in abrupt changes of the tensor order parameter [13].

IV. RESULTS AND DISCUSSIONS

A. Phase-plane analysis of cholesteric order

Ordinary nematic liquid-crystalline materials are characterized by their uniaxiality, whose amplitude and intensity are directly related to the value of the thermodynamic potential—i.e., temperature or concentration. In the case of cholesteric mesophases (chiral nematics), the situation is somewhat more complicated since the symmetry of the structure is a function of the helical pitch. The importance of this length scale on the symmetry of the mesophase is captured by a phase-plane analysis of the system of equations (8a) and (8b).

Figure 2 exhibits all possible orientation states in the scalar order parameter S-P triangle for a given parametric choice. The states described are as follows [14]: (a) isotropic state (the three eigenvalues of **Q** are identical): $S=0$ and $P=0$; (b) uniaxial state (two eigenvalues of **Q** are identical): (i) line $P=0$, (ii) line $P=3S$, and (iii) line $P=-3S$; and (c) biaxial state (the three eigenvalues of **Q** are distinct): $S\neq0$ and $P\neq0$, interior of the order parameter triangle excluding the three uniaxial lines.

In addition to this atlas of ordering states, Fig. 2 gives the seven stationary points corresponding to the steady-state solutions for the autonomous system given by Eqs. (8a) and (8b) for $U=6$ and $\xi/p_0=0.03$ (the pitch p_0 is 33.33 times longer than the coherence length). The dashed lines indicated nullclines. The three nodal sinks (SI) give the value of the equilibrium scalar order parameters S and P. In simulations, the system always picks up the attractor located on the $S>0$ part of the plane, since uniaxiality prevails over biaxiality in this system. The nodal source (SO) corresponds to the unstable isotropic source. The remaining saddle points (SA) are unstable solutions corresponding to defects that the system might encounter in the presence of orientational incompatibilities [15]. The chirality (ξ/p_0) forces the system to

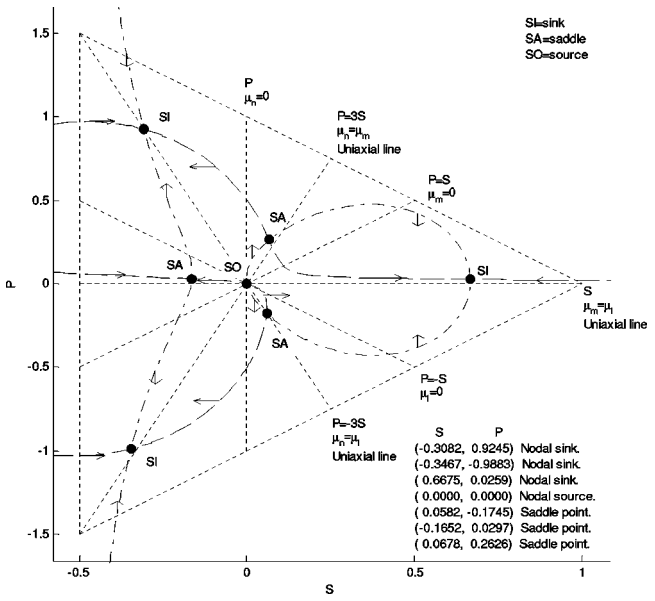

FIG. 2. Atlas of the orientation states in the scalar order parameter S-P triangle and steady-state solutions to the autonomous system given by Eq. (10). The orientation states are isotropic-state node ($S=0$,$P=0$); uniaxial-state (i) line $P=0$, (ii) line $P=3S$, and (iii) line $P=-3S$; biaxial state in the interior of the triangle excluding the three above mentioned uniaxial lines. The black dots represent the seven stationary points characterizing the symmetry of the cholesteric mesophase for $U=6$ and $\xi/p_0=0.03$. The three nodal sinks (SI) give the value of the equilibrium scalar order parameters S and P. The nodal source (SO) corresponds to the unstable isotropic source. The saddle points (SA) are unstable solutions corresponding to defects that the system might encounter in the presence of orientational incompatibilities.

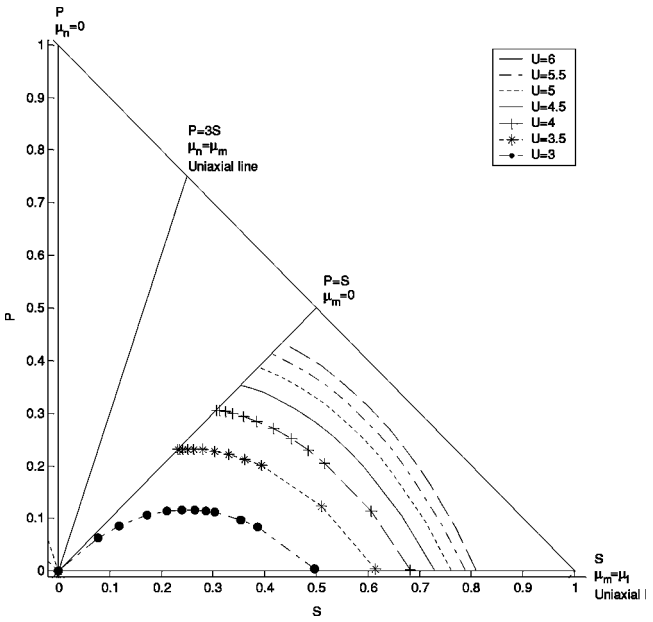

FIG. 3. Computed trajectories of the cholesteric sink node, as ξ/p_0 increases from 0.01 to 1. Each of the seven trajectories corresponds to a given value of U. As U increases, the trajectories shift upwards in the S-P triangle. The start of each trajectory is the nearly uniaxial state ($P\approx 0$) and the end is the maximally biaxial line ($P=S$). When $U=3$ (the limit of metastability of the ordinary nematic), the increase of ξ/p_0 brings the stable state to the isotropic node.

slightly deviate from the uniaxial symmetry, characteristic of ordinary achiral nematics.

The asymptotic behavior of the numerical solutions to Eqs. (8) can be used to establish the role of biaxiality in cholesteric phases and therefore, by analogy, in biological plywoods. Figure 3 shows seven computed trajectories of the cholesteric sink node, as ξ/p_0 increases from 0.01 to 1. Each of the seven trajectories corresponds to a given value of U (see legend to Fig. 3). As U increases, the trajectories shift upwards in the S-P triangle. The start of each trajectory is the nearly uniaxial state ($P\approx 0$) and the end is the maximally biaxial line ($P=S$). When $U=3$ (the limit of metastability of the ordinary nematic), the increase of ξ/p_0 brings the stable state to the isotropic node. In other words, ξ/p_0 modifies the metastability limit of the cholesteric phase. The uniaxial line $P=0$, corresponds to the solutions that minimize the short-range energy while the solutions on the (maximally) biaxial line $P=S$ minimize the long-range contribution. For a certain value of the ratio ξ/p_0, the balance between short- and long-range effects shifts and the most stable conformation for the system becomes the so-called blue phase in which helicity is not restrained to lie on one plane [10]. This complicated structure is not accessed in our study since the physical values of ξ/p_0 are expected to be such that the solution nodes tend towards the $P=0$ line, where the stable phase is found to be cholesteric with a non-minimized gradient energy. However, the blue-phase architecture has been identified in biological composites [1] and is relevant in many other biological systems such as DNA solutions [16]. This simple phase-plane analysis of the reduced governing equations allows an understanding of the symmetry properties of these chiral assemblies at steady state.

B. Formation of the planar monodomain twisted plywood architecture

This section presents representative simulation results describing the formation process of the planar monodomain twisted plywood architecture found in both cholesteric liquid crystals and biological fibrous composites [1]. For direct visualization of the tensor order parameter field $\mathbf{Q}(x,y,t)$, we draw parallelepipeds which render possible the simultaneous representation of orientation and alignment information. These parallelepipeds are defined with the eigensystem of $\mathbf{Q}$ [17,18]; the three eigenvectors ($\mathbf{n}$,$\mathbf{m}$,$\mathbf{l}$) give the orientation of the parallelepipeds and the corresponding three eigenvalues $[\lambda_{\mathbf{n}}=2/3S,\lambda_{\mathbf{m}}=-1/3(S-P),\lambda_{\mathbf{l}}=-1/3(S+P)]$ give the degree of alignment along these orientation directions. Since the eigenvalues of $\mathbf{Q}$ span the interval $[-1/3,2/3]$, they are augmented by 1/3 so as to span the interval $[0,1]$. Therefore, the microstructure of the material is depicted by the shifted tensor $\mathbf{M}=\mathbf{Q}+\boldsymbol{\delta}/3$, as shown Fig. 4. Using this technique, an isotropic state is represented by a small cube. A uniaxial state is represented by a parallelepiped with two edges of same length and a biaxial state by a parallelepiped with three edges of different lengths.

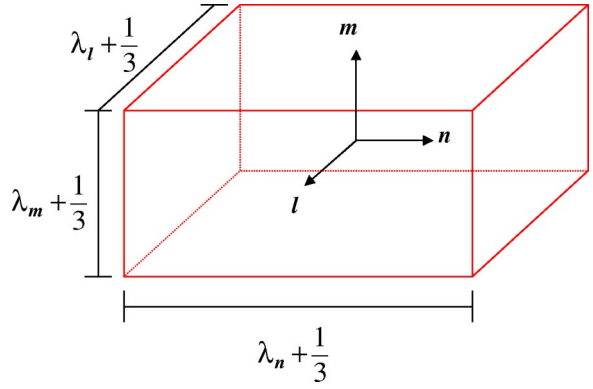

FIG. 4. Representation of microstructure by the shifted tensor $\mathbf{M}=\mathbf{Q}+\boldsymbol{\delta}/3$. The parallelepipeds are constructed with the eigensystem of $\mathbf{Q}$; the three eigenvectors ($\mathbf{n},\mathbf{m},\mathbf{l}$) giving the orientation and the three eigenvalues ($\lambda_\mathbf{n},\lambda_\mathbf{m},\lambda_\mathbf{l}$) augmented by 1/3 giving the degree of alignment. An isotropic state is represented by a small cube. A uniaxial state is represented by a parallelepiped with two edges of same length and a biaxial state by a parallelepiped with three edges of different lengths.

Since the effect of elastic anisotropy is out of scope in this study, we use the one-constant approximation $\upsilon=1$ that renders the splay, the twist, and the bend modes of deformation [6] indistinguishable and simplifies the long-range contribution of the governing equation as follows:

$$\mathrm{LR}=-\left(\frac{\xi}{h_0}\right)^2[\nabla^2\cdot\mathbf{Q}]+\left(\frac{\xi}{h_0}\right)\left(\frac{\xi}{p_0}\right)[-8\pi(\nabla\times\mathbf{Q})]^{[s]}+\left(\frac{\xi}{p_0}\right)^2[-16\pi^2\mathbf{Q}]. \tag{10}$$

Figure 5 shows a time series of the tensor field $\mathbf{M}(x,y,t)$ describing the propagation of order in the material, for $U=6$, $\xi/p_0=0.03$, and $\xi/h_0=0.015$. (For this representative simulation the dimensionless pitch is therefore equal to 1/2.) The computational grid has 301 nodes in the x and y directions. When the thermodynamic potential U (proportional to concentration of fibrous molecules in the extracellular matrix) increases from $U<8/3$ to $U=6$, the homogenous isotropic state becomes unstable and a nonlocal spontaneous phase-ordering process starts. Strong gradients of order (S and P) are created between the initial constraining layer at $y=0$ and the isotropic material bulk. Recall that at $y=0$, (S,P) are the stable biaxial steady-state solutions to Eqs. (10). As a result, order and orientation are induced in the unstable isotropic bulk of the material and converted into a stable cholesteric phase. Figure 5(a) shows a field of randomly oriented cuboids representing the initial isotropic state of the material. Figures 5(b) and 5(c) depict the time evolu-

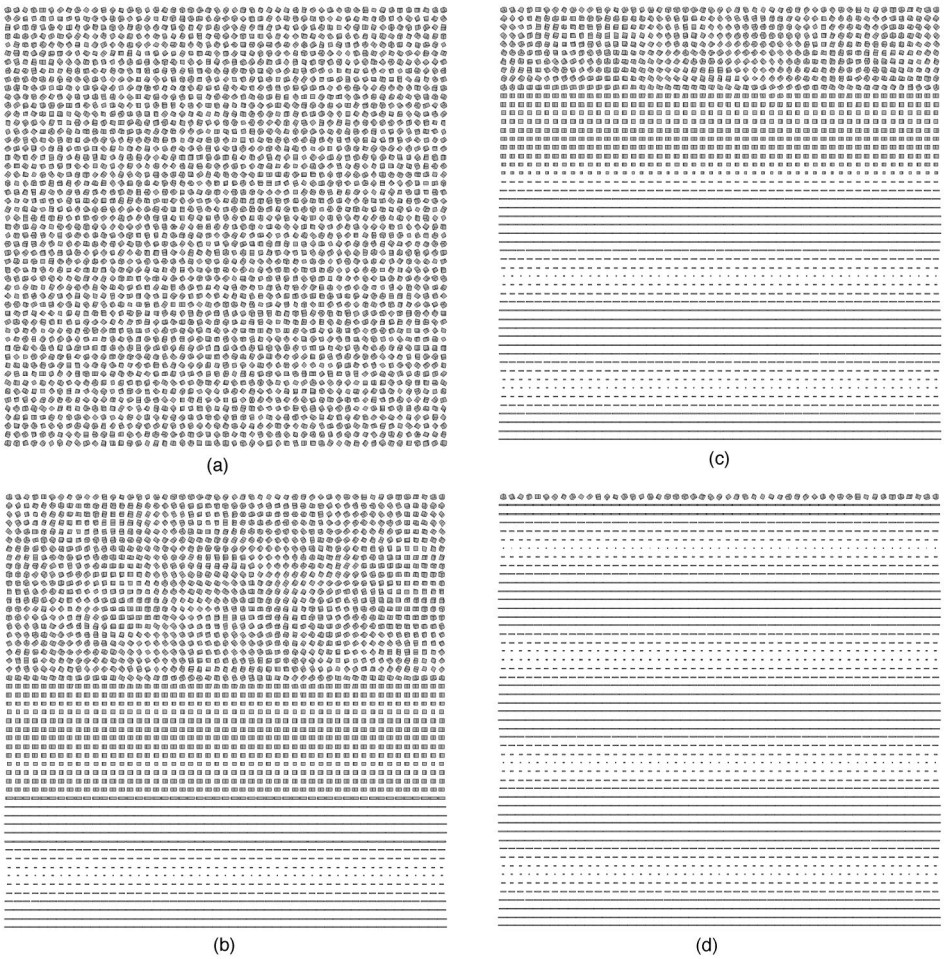

FIG. 5. Time evolution of the microstructure. (a) Field of randomly oriented cuboids representing the initial isotropic state of the material. (b),(c) Order progresses as a moving front from the stable initial constraining layer and leaves behind a fully relaxed helical microstructure. (d) Steady-state microstructure of the material corresponding to the planar monodomain cholesteric structure analogous to the twisted plywood architecture. The absence of topological defects is due to the fact that there is unique helical direction for the whole material. The specific times are 0 (a), 10 (b), 20 (c), 30 (d). Boxes are of unit length.

tion of the microstructure. Order progresses as a moving front from the stable initial constraining layer and leaves behind it a fully relaxed helical microstructure. The ordered material exhibits a single helical direction (**N**) that is perpendicular to the moving front (and the surface of structure in formation). The material remains homogeneous in the x direction perpendicular to the front. Once established, the defect-free cholesteric order is stable and no further reorientation mechanisms occur in its wake. Figure 5(d) gives the steady-state microstructure of the material corresponding to the planar monodomain cholesteric structure analogous to the twisted plywood architecture. The absence of topological defects is due to the fact that there is a unique helical direction (**N**) for the whole material and therefore no orientational incompatibilities between neighboring regions exist. Knowing that the microstructure of the bulk is greatly affected by the limiting surfaces and therefore this ''ideal'' arrangement of the molecules within the material is due to the specific anchoring of the molecules on the physical boundaries.

Periodic boundary conditions have been employed on the x direction in order to remove surface effects from the sides. The upper boundary of the computational domain represents the surface of the secreting cell along which the fibrous molecules are isotropically ordered. Hence, the only physical boundary that can act on the material bulk is the previously solidified ordered layer (lower boundary of the computational domain). Along this initial constraining layer, the molecules describe a smooth (the director orientation is perfectly regular) planar (molecules parallel to the surface) state, the system naturally adopts its helical direction (**N**) perpendicularly to the restraining surface. It is understood here that if the domain were to be expanded—i.e., as would be expanded in a biological system—this boundary would be ordered exactly like its predecessor and serve as the new initial constraining layer in the expansion cycle of the biological composite. Therefore, by analogy, the monodomain twisted architecture of biological fibrous composites is assumed to arise through an ordering process qualitatively similar to the one described above, in which a planar anchoring of the chiral molecules at the surface is indispensable.

Figure 6 shows the time evolution of the uniaxial scalar order parameter S (degree of alignment) and the out-of-plane component $|n_z|$ of the director field using gray scale intensity plots, for the same parametric values and dimensionless times used in the simulations results shown in Fig. 5. The fields go from white to black as the scalar order parameter goes from its equilibrium value to zero, and the out-of-plane component $|n_z|$ goes from 0 to ± 1. From Fig. 6, it is clear that both order (S) and orientation $|n_z|$ propagate as fronts. Both fronts have the same speed, but the director front precedes the scalar order front parameter. This is not surprising as an increase in alignment—i.e., the scalar order parameter—requires a well-established average director orientation. In other words, the distance that separates the fronts of the two processes corresponds to a preoriented layer. Therefore the phase-ordering process consists first of the establishment of orientation and then an increase of alignment along the direction adopted by the system. The thickness of the preorientation layer corresponds (roughly) to the half-cholesteric pitch. In addition to the lag, Figs. 6(b), 6(d), and 6(f) illustrate the periodic extinction of light that characterizes the twisted plywood architecture observed in polarized light microscopy and that arises every half-cholesteric pitch.

Figure 7 shows the time evolution of the scalar order parameters S and P along the helix direction (**N**). The picture shows that the initial shape of the front is conserved. Also, the speed of the front is constant and the degree of biaxiality is very low compared to the degree of uniaxiality. The small overshoot in the biaxial order parameter profiles is explained by the nonlinearity of the front. Since P is coupled to S and its gradient, the highest value of P appears at the highest value in the gradient of S. This is easily seen by the arced trajectory made by the front in the S-P triangle (Fig. 8).

C. Kinetics of the phase-ordering process

In this section, we focus on the kinetics of the ordering-process that leads to the planar monodomain twisted plywood. The objective is to get a sense of the speed of this process with respect to the thermodynamic potential U and the length scale ratios ξ/p_0 and ξ/h_0 (material properties).

In order to do this, we assume that the cholesteric liquid crystal is uniaxial (this is justified by the strong uniaxiality that prevails over biaxiality in the cholesteric geometry). Also, we assume that the director **n** is fixed in time and that it describes an ideal helix along the normal to the interface (this is justified by the observation that, in the simulations, the kinetics of the moving front are unaffected by the director triad orientation). Given these simplifying assumptions, the original problem reduces to a one-dimensional time-dependent Ginzburg-Landau (TDGL) type of equation [19–21].

The TDGL equation associated with the present problem reads

$$\frac{\partial S}{\partial t}-\left(\frac{\xi}{h_0}\right)^2\frac{\partial^2 S}{\partial y^2}=-\frac{\partial f}{\partial S}=\left[-1+\frac{1}{3}U-4\pi^2\left(\frac{\xi}{p_0}\right)^2\right]S+\frac{1}{3}US^2-\frac{2}{3}US^3. \tag{11}$$

Equation (11) accepts two types of topological solutions. The first type of solutions interpolating between a local maximum and a minimum of the free energy potential $f(S)$ are called relaxation modes. These traveling-wave solutions have a multitude of possible velocities. A second type of traveling-wave solutions, interpolating between two minima of the free energy potential $f(S)$, are called domain wall solutions (or interface layers). These solutions have a velocity uniquely determined by the form of the free energy potential $f(S)$ and by the boundary conditions [22]. We are therefore interested in the latter solution, which are time- and space-dependent traveling-wave solutions corresponding to the roots of the free energy potential $f(S)$. Although solutions to Eq. (12) are well known for the case of an infinite pitch p_0 (i.e., achiral nematics) [19–21], the presence of chirality $(p_0 \neq 0)$ introduces new significant effects that have not been established or explained.

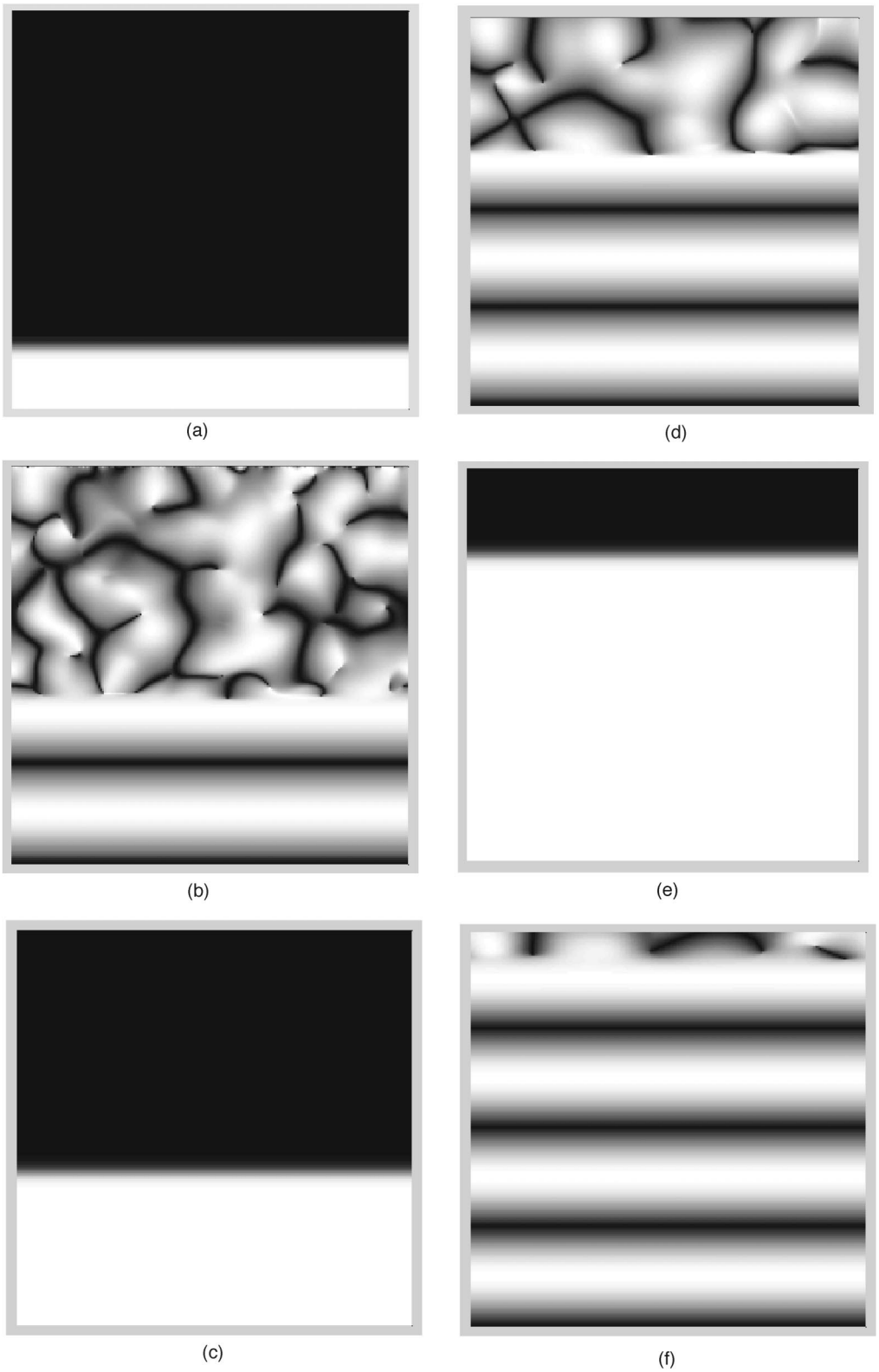

FIG. 6. Time evolution of the uniaxial scalar order parameter S (left) and the out-of-plane component $|n_z|$ of the director field (right) using gray scale intensity plots. The fields go from white to black as the scalar order parameter goes from its equilibrium value to zero and the out-of-plane component $|n_z|$ goes from 0 to ± 1. The specific time are 5 (a),(b); 12.5 (c),(d); 25 (e),(f). Alignment (S) and orientation $|n_z|$ propagate as fronts of equal speeds; however, the scalar order front parameter lags the director front, because to grow S needs a well-established average orientation. The thickness of the preorientation layer corresponds (roughly) to the half-cholesteric pitch. The periodic extinction of light arises every half-cholesteric pitch. Boxes are of unit length.

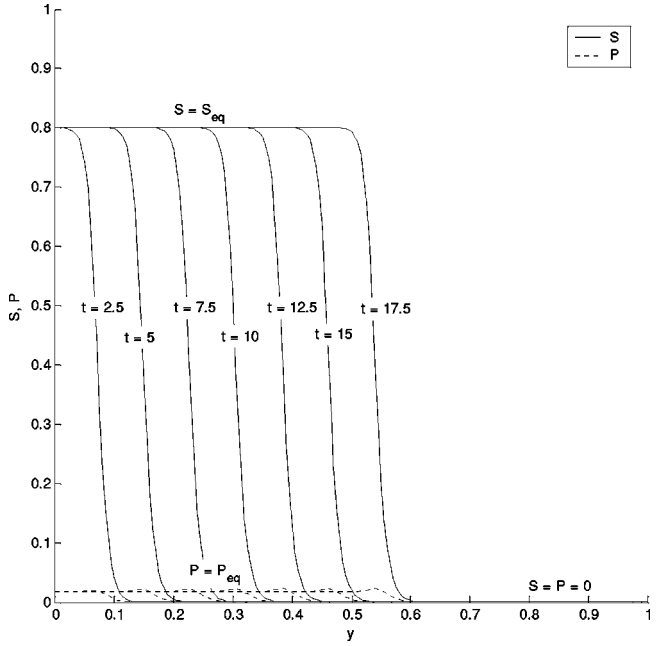

FIG. 7. Time evolution of the scalar order parameters S and P along the helix direction. The initial shape of the front is conserved and its speed is constant. The degree of biaxiality is very low compared to the degree of uniaxiality.

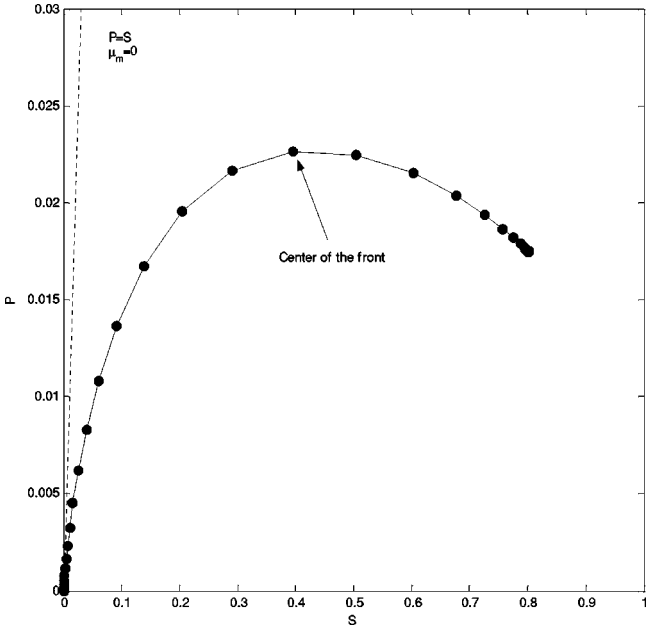

FIG. 8. Trajectory of the scalar order parameters through the interface in the S-P triangle. The nonlinearity of the front clearly appears from the arced trajectory.

To establish phase stability of this system we follow the standard approach of [9]. In order to determine the critical values of U and ξ/p_0 for the phase transition between the isotropic and cholesteric phases, we use the following free energy potential:

$$f=\left[\frac{1}{2}-\frac{1}{6}U+2\pi^2\left(\frac{\xi}{p_0}\right)^2\right]S^2-\frac{1}{9}US^3+\frac{1}{6}US^4. \quad (12)$$

Similar to achiral nematic liquid crystals [9], there are four characteristic stability regions, limited by three critical thermodynamic potential U^{**}, U_{IC}, and U^*, as follows.

(i) $U<U^{**}$: the system has one global minimum corresponding to $S=0$, so that the isotropic phase is stable and the ordered $(S\neq 0)$ phase is unstable. The thermodynamic potential $U=U^{**}$ corresponds to the limit of metastability for the cholesteric ordered phase.

(ii) $U^{**}<U<U_{\mathrm{IC}}$: the free energy exhibits two minima: the global/stable minimum corresponds to the disordered phase while the local/metastable minimum belongs to the ordered phase. U_{IC} designates the thermodynamic potential at which the isotropic-cholesteric phase transition occurs; at this particular potential, the free energy is equivalently minimized by the isotropic and ordered phases and therefore both are stable. This equivalence characterizes the first-order discontinuous phase transition.

(iii) $U_{\mathrm{IC}}<U<U^*$: the ordered phase becomes the global/stable minimum of free energy while the isotropic state represents a local/metastable minimum. The thermodynamic potential U^* marks the metastability limit of the isotropic phase.

(iv) $U^{**}<U$: the only stable phase becomes the ordered one.

The values of these critical thermodynamic potentials U_{IC}, U^{**}, and U^* are

$$U_{\mathrm{IC}}=2.7\left[1+4\pi^2\left(\frac{\xi}{p_0}\right)^2\right], \quad (13a)$$

$$U=\frac{8}{3}\left[1+4\pi^2\left(\frac{\xi}{p_0}\right)^2\right], \quad (13b)$$

$$U^*=3\left[1+4\pi^2\left(\frac{\xi}{p_0}\right)^2\right]. \quad (13c)$$

When $p_0\rightarrow\infty$ we recover the well-known achiral nematic results [11]. As apparent from Eqs. (13), the critical potentials U_{IC}, U^{**}, and U^* that are, respectively, 2.7, 8/3, and 3 for achiral nematics are now amplified by $[1+4\pi^2(\xi/p_0)^2]$. Thus, to form a chiral nematic phase, a higher concentration of rodlike molecules is required than for an achiral one. The thermodynamic potential dependence of the equilibrium order parameter $S(U)$ for different values of the ratio ξ/p_0 is given in Figs. 9(a)–9(d). The vertical lines indicate the critical thermodynamic potentials determining the stability of the isotropic and cholesteric phases. The solid and dotted lines indicate, respectively, stable and metastable states of the given phase. The overall shape of the initial profile is conserved as ξ/p_0 is increased; $S(U^{**})=1/4$, $S(U_{\mathrm{IC}})=1/3$, and $S(U^*)=1/2$.

We next analyze traveling-wave solutions to Eq. (11). Using a front comoving frame, the scalar order parameter becomes

$$S(y,t)=S(y-vt)=S(y'), \quad (14)$$

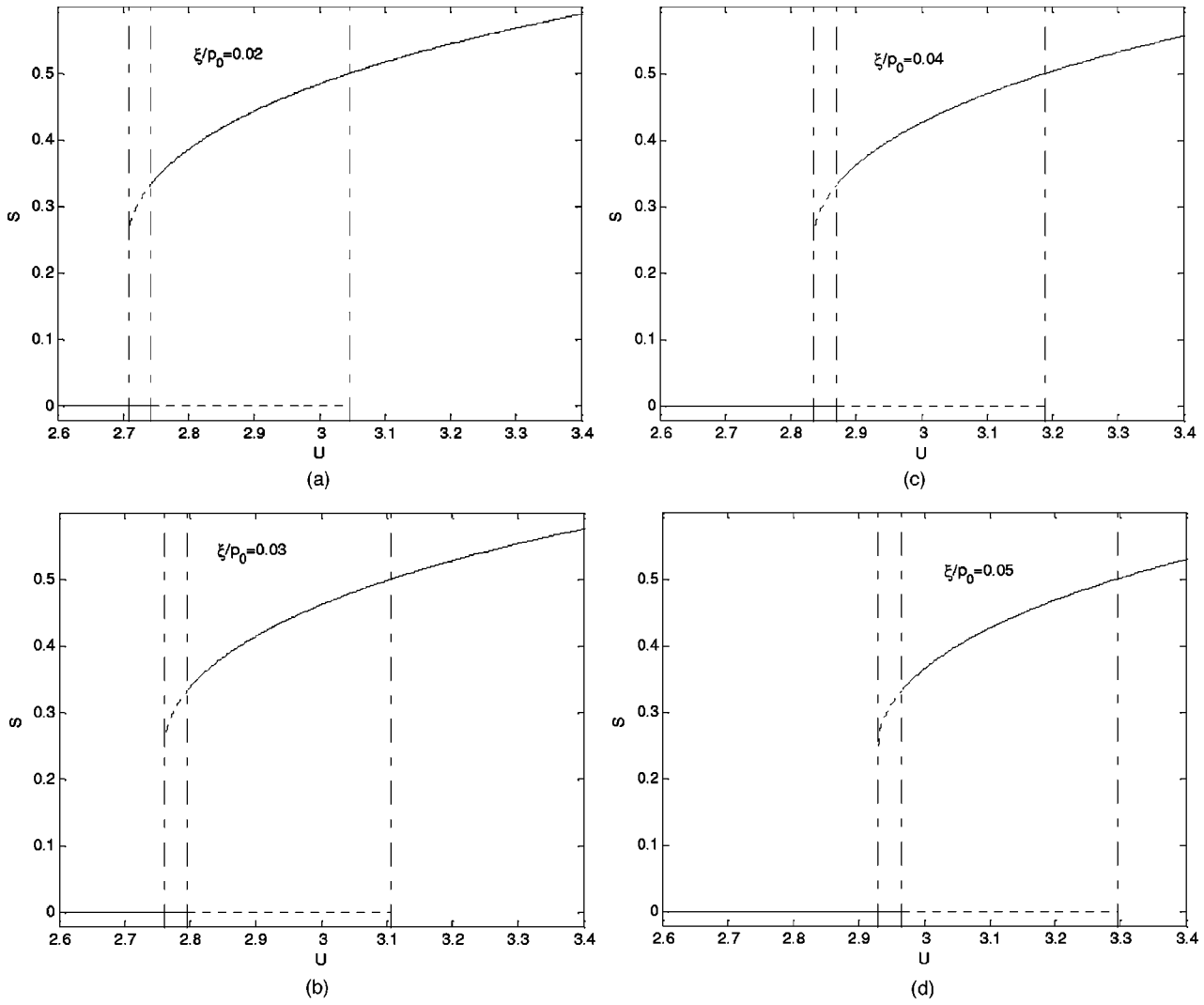

FIG. 9. Dependence of the equilibrium order parameter S for different values of the ratio ξ/p_0. The vertical lines indicate the critical thermodynamic potential that rule stability of the isotropic and cholesteric phases. The solid and dotted lines indicate, respectively, stable and metastable states of the given phase. The overall shape of the initial profile is conserved as ξ/p_0 is increased.

where v is the velocity of propagation in the y direction of the traveling-wave solution. Rewriting Eq. (11) using Eq. (14) leads to the following ordinary differential equation:

$$v\frac{\partial S}{\partial y'}+\left(\frac{\xi}{h_0}\right)^2\frac{\partial^2 S}{\partial y'^2}=\frac{\partial f}{\partial S}=\left[1-\frac{1}{3}U+4\pi^2\left(\frac{\xi}{p_0}\right)^2\right]S-\frac{1}{3}US^2+\frac{2}{3}US^3. \tag{15}$$

The right-hand side of Eq. (15) can be written as

$$\frac{df}{dS}=A_2S+A_3S^2+A_4S^3, \tag{16}$$

$$A_2=\left[1-\frac{1}{3}U+4\pi^2\left(\frac{\xi}{p_0}\right)^2\right],\quad A_3=-\frac{1}{3}U,\quad A_4=\frac{2}{3}U, \tag{17}$$

and the roots of the polynomial df/dS are given by

$$S_1=0, \tag{18a}$$

$$S_2=\frac{1}{4}-\frac{1}{4}\sqrt{9-\frac{24}{U}-\frac{96}{U}\pi^2\left(\frac{\xi}{p_0}\right)^2}, \tag{18b}$$

$$S_3=\frac{1}{4}+\frac{1}{4}\sqrt{9-\frac{24}{U}-\frac{96}{U}\pi^2\left(\frac{\xi}{p_0}\right)^2}. \tag{18c}$$

The solutions S_1 and S_3 correspond, respectively, to the isotropic and cholesteric minima of the free energy potential f. The solution S_2 is related to a maximum of the free energy functional. As apparent from Eq. (18c), the equilibrium scalar order parameter of the cholesteric phase depends not only on the thermodynamic potential (like achiral nematic) but also on the ratio between the internal length scale and the pitch. Since the solution of interest here is the interface layer or domain wall between the cholesteric and isotropic phases, moving at a velocity v, Eq. (15) is subject to the boundary

conditions $S(-\infty)=S_3$ and $S(+\infty)=S_1$. Following the steps of [19–24], Eq. (15) is rewritten using the solutions S_1, S_2, and S_3:

$$v\frac{dS}{dy'}+D\frac{d^2S}{dy'^2}-A_4(S-S_1)(S-S_2)(S-S_3)=h(S)=0, \tag{19}$$

with

$$D=\frac{2}{3}\left(\frac{\xi}{h_0}\right)^2. \tag{20}$$

We know that the two minima of $f(S)$ are S_1 (corresponding to the isotropic phase) and S_3 (corresponding to the cholesteric phase). Consequently, we assume that the scalar order parameter S satisfies the differential equation

$$\frac{dS}{dy'}=K(S-S_1)(S-S_3), \tag{21}$$

where K is an unknown function of the equation parameters. Deriving an analogous relation for the second-order differential equation in the scalar order leads to

$$\frac{d^2S}{dy'^2}=\frac{d}{dy'}\left(\frac{dS}{dy'}\right)=\left[\frac{d}{dS}\left(\frac{dS}{dy'}\right)\right]\frac{dS}{dy'}$$
$$=K^2(S-S_1)(S-S_3)(-S_1+2S-S_3). \tag{22}$$

Replacing the above relations Eqs. (21) and (22), into Eq. (19) leads to the following algebraic relation:

$$(S-S_1)(S-S_3)\{(2DK^2-A_4)S-[DK^2(S_1+S_3)-A_4S_2$$
$$-vK]\}=h(S)=0. \tag{23}$$

The function $h(S)$ will be zero if

$$(2DK^2-A_4)=0, \tag{24a}$$

$$[DK^2(S_1+S_3)-A_4S_2-vK]=0. \tag{24b}$$

These two former relations determine K and the wave velocity v as

$$K=\sqrt{\frac{U}{3}}\left(\frac{\xi}{h_0}\right)^{-1}, \tag{25}$$

$$v=\sqrt{\frac{U}{3}}\left(\frac{\xi}{h_0}\right)\left[-\frac{1}{4}+\frac{3}{4}\sqrt{9-\frac{24}{U}-\frac{96}{U}\pi^2\left(\frac{\xi}{p_0}\right)^2}\right]. \tag{26}$$

The solution of Eq. (21) satisfies the full equation (15) if K and v are given by the above relations (25) and (26). The speed of the traveling wave turns out to depend on all the different parameters of Eq. (15). The actual solution $S(y')$ is obtained by solving Eq. (21) which gives the classical front solution [19–24]

$$S(y')=\frac{S_3}{2}\left\{1-\tanh\left[K\frac{S_3}{2}y'\right]\right\}. \tag{27}$$

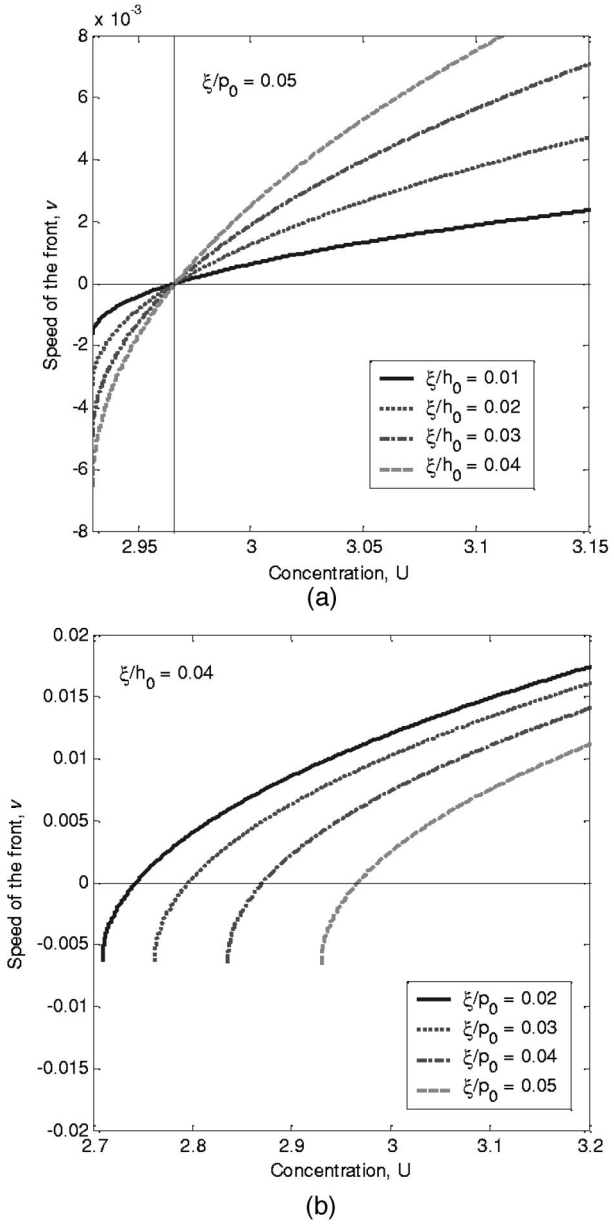

FIG. 10. Behavior of the traveling ordering interface. (a) When $U>U_{IC}$, the speed of the front is positive as the stable cholesteric phase is advancing into the isotropic metastable/unstable phase. However, when $U<U_{IC}$, speed is negative and the isotropic front is advancing. At the exact thermodynamic potential $U=U_{IC}$ the interface becomes static. The speed increases with the ratio ξ/h_0. (b) When the ratio ξ/p_0 increases, the speed decreases (for any given thermodynamic potential).

Solution (27) has a front shape which connects the two nondegenerate minima of the free energy potential. It describes the domain wall between the two phases, moving at the velocity v. The velocity is unique because it corresponds to the case where the potential difference between the two phases is exactly compensated by dissipation. Hence, solution (27) is a power balanced solitary wave or diffusive soliton [23].

Equation (27) yields a positive velocity as long as $U>U_{IC}$ which indeed confirms that the stable cholesteric

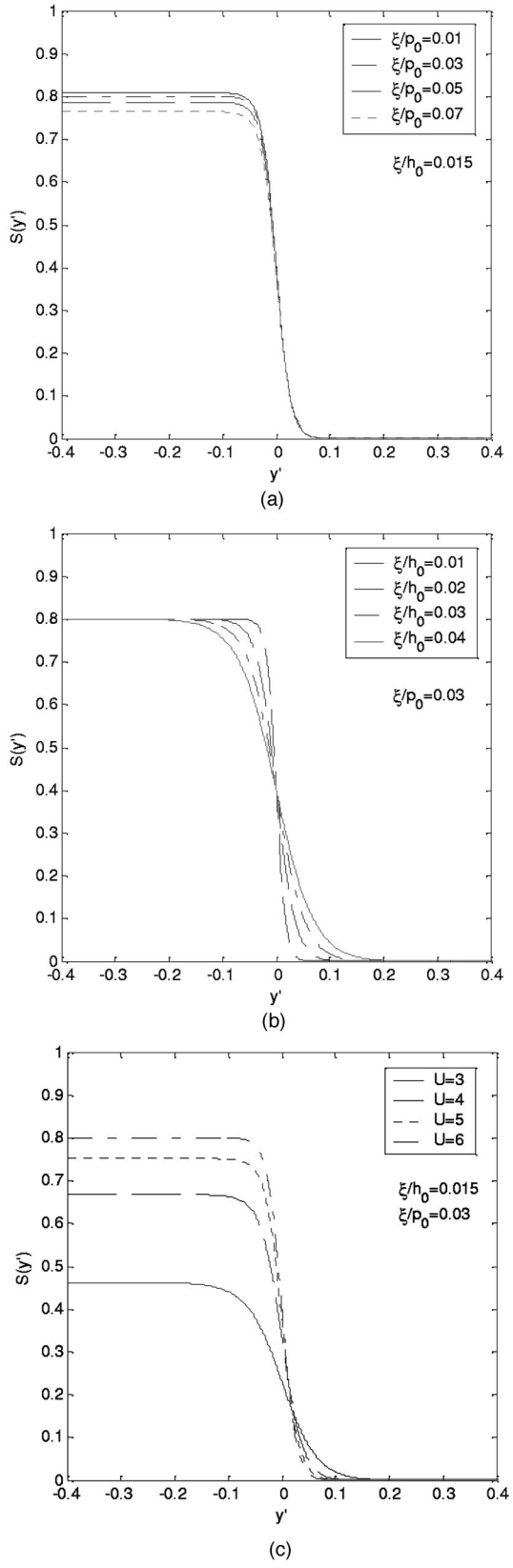

FIG. 11. Response of the scalar order parameter profile for an increase of (a) ξ/p_0, (b) ξ/h_0, and (c) U. The amplitude of the front is affected by the pitch (p_0) and by the thermodynamic potential (U), while the shape of the front is affected by both thermodynamic potential and coherence (ξ) length.

phase is advancing into the isotropic metastable/unstable phase. Similarly, if $U<U_{\mathrm{IC}}$, the velocity is negative and the isotropic is advancing. At the exact thermodynamic potential $U=U_{\mathrm{IC}}$ the interface becomes static. In addition, when the ratio between the internal and external length scales, ξ/h_0, increases, the speed of the front increases too. However, when the ratio between the internal length scale and the pitch, ξ/p_0, increases, the speed decreases (for any given thermodynamic potential). So the speed profiles shift in a similar way to the scalar order parameter profiles. Since it has been established previously from the phase-plane analysis of the original governing equation that an increase in the ratio ξ/p_0 leads to an increase in the biaxial ordering, it is concluded here that an increase in biaxiality of the ordered phase reduces its speed of progression. Figures 10(a) and 10(b) summarize the behavior of the traveling ordering interface.

Additionally, it is found that the shape of the scalar order parameter profile at the interface is flattened by an increase of the ξ/p_0 ratio; this result is consistent with the observation that as biaxiality increases, uniaxiality decreases. The thickness of the interface reduces with the ξ/h_0 ratio, which is again consistent with physically observed behavior. Looking now at the effect of the thermodynamic potential (U), the two previous phenomena are observed to occur at the same time. That is, as the thermodynamic potential (U) increases, the interface thickness shrinks and the equilibrium order parameter of the stable cholesteric phase increases.

Figures 11(a)–11(c) show the behavior of the scalar order parameter profile across the interface. The figures show that the amplitude of the front is affected by the pitch (p_0) and by the thermodynamic potential (U), while the shape of the front is affected by both the thermodynamic potential and coherence (ξ) length. To assess the usefulness of the uniaxial solution (28) we next determine its accuracy. Figure 12 compares the shape of the computed front [numerical solutions to Eqs. (6)] with the analytical solution (27). The figure shows that even in the presence of an induction time for the computational solution, the front position at a representative time of $t=17.5$ is almost identical. The front shape for both cases is also very close. Thus, we conclude that for sufficiently large pitches, the analytical results obtained under the uniaxial approximation compare well with the numerical results of the governing equation and therefore are useful to describe the parametric sensitivity of chiral front propagation in cholesteric phases such as those found in the matrix of a developing biological fibrous composite.

V. CONCLUSIONS

A model based on the Landau–de Gennes theory has been used to simulate a lyotropic cholesteric liquid-crystalline material in order to understand the structure formation process of the twisted plywood architecture ubiquitously found in biological fibrous composites. The model is able to reproduce the experimentally observed planar monodomain textures. The numerical simulations confirm that, as suggested by Neville [1], a constraining layer is necessary for the structure to have a unique helical axis and be monodomain. The

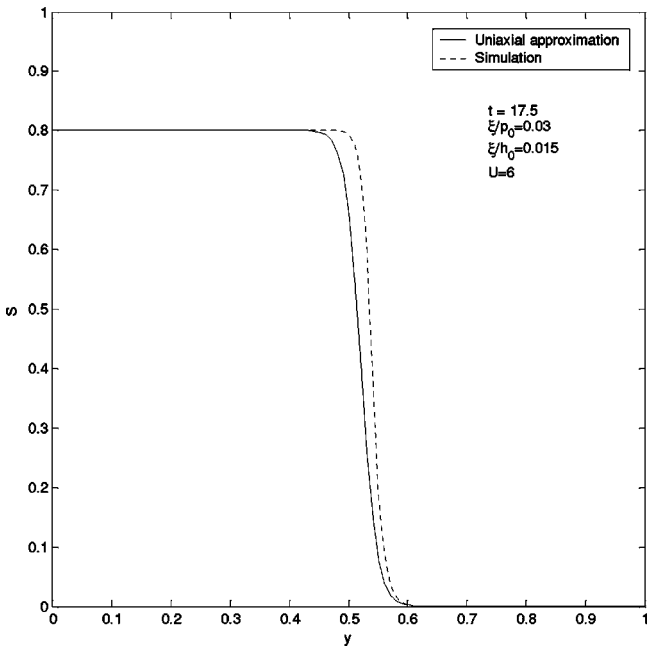

FIG. 12. Comparison of the front from numerical solutions and uniaxial approximation at the representative time $t=17.5$. The shape and position of the front are also very close which assesses the relevance of the uniaxial solution.

absence of such a preordered layer leads otherwise to multiple helical axes and therefore to polydomain textures with topological defects that weaken the mechanical integrity of the structure.

A phase-plane analysis of the reduced governing equation reveals that biaxiality increases with the ratio between the internal length scale and the cholesteric pitch, ξ/p_0 (its chirality). Since biological fibrous composites are long-pitch systems, their structure is essentially uniaxial.

Finally, an analysis made under the assumption of a uniaxial cholesteric mesophase showed how the different parameters of the model affect the speed of the ordering process. As expected, the speed of the ordering process was found to increase with the thermodynamic potential and the ratio ξ/h_0. However, the process is slowed by an increase in chirality. This deceleration of the ordering process is in turn linked to the increase of the biaxiality generated by the increased chirality of the material as shown in the *S*-*P* triangle. This means that the symmetry of the phase and its asymmetric fibrous constituents greatly influences the time required for the biological composite to assemble itself. Finally, the thickness of the dynamic domain wall shrinks with an increase in the thermodynamic potential and a decrease of the ratio ξ/h_0.

We hope that these results will contribute to a better understanding of the mechanisms which control the formation of the planar monodomain twisted plywood architecture found in cholesteric liquid crystals and their biological fibrous composite analogs.

ACKNOWLEDGMENTS

This work was supported by a grant from the Donors of The Petroleum Research Fund (PRF) administered by the American Chemical Society.

[1] C. Neville, *Biology of Fibrous Composites* (Cambridge University Press, Cambridge, England, 1993).
[2] Y. Bouligand, in *Liquid Crystalline Order in Polymers*, edited by A. Blumestein (Academic Press, New York, 1978).
[3] M.M. Giraud-Guille, Calcif. Tissue Int. **42**, 167 (1988).
[4] M.M. Giraud-Guille, Int. Rev. Cytol. **166**, 59 (1996).
[5] M.M. Giraud-Guille, Curr. Opin. Solid State Mater. Sci. **3**, 221 (1998).
[6] S.C. Cowin, J. Biomed. Eng. **122**, 533 (2000).
[7] M. Elices, *Structural Biological Materials: Design and Structure-Property Relationships* (Pergamon, New York, 2000).
[8] A.L. Koch, *Bacterial Growth and Form* (Chapman & Hall, London, 1995).
[9] P.G. de Gennes and J. Prost, *The Physics of Liquid Crystals*, 2nd ed. (Oxford University Press, New York, 1993).
[10] D.C. Wright, N.D. Mermin, Rev. Mod. Phys. **61**, 385 (1989).
[11] M. Doi and S.F. Edwards, *Theory of Polymer Dynamics* (Oxford University Press, New York, 1987).
[12] T. Tsuji and A.D. Rey, Macromol. Theory Simul. **7**, 623 (1998).
[13] P.J. Van der Houwen, Appl. Numer. Math. **20**, 261 (1996).
[14] A.D. Rey, Macromol. Theory Simul. **4**, 857 (1995).
[15] D. Walgraef, *Spatio-Temporal Pattern Formation With Examples from Physics, Chemistry, and Materials Science* (Springer-Verlag, Berlin, 1996).
[16] F. Livolant and A. Leforestier, Prog. Polym. Sci. **21**, 1115 (1996).
[17] A. Sonnet, A. Kilian, and S. Hess, Phys. Rev. E **52**, 718 (1995).
[18] S. Mkaddem and E.C. Gartland, Phys. Rev. E **62**, 6694 (2000).
[19] V. Popa-Nita and T.J. Sluckin, J. Phys. II **6**, 873 (1996).
[20] V. Popa-Nita, T.J. Sluckin, and A.A. Wheeler, J. Phys. II **7**, 1225 (1997).
[21] V. Popa-Nita, Mol. Cryst. Liq. Cryst. Sci. Technol., Sect. A **257**, 141 (1994).
[22] M. Otwinowski, J.A. Tuszynski, and J.M. Dixon, Phys. Rev. A **45**, 7263 (1992).
[23] M. Remoissenet, *Waves Called Solitons, Concepts and Experiments*, 3rd ed (Springer, Berlin, 1999).
[24] J.D. Murray, *Mathematical Biology* (Springer-Verlag, Berlin, 1990).